JACS
JOURNAL OF THE AMERICAN CHEMICAL SOCIETY
Article
pubs.acs.org/JACS

Comprehensive Spectroscopic Determination of the Crystal Field Splitting in an Erbium Single-Ion Magnet

Yvonne Rechkemmer,[†] Julia E. Fischer,[†,⊥] Raphael Marx,[†] María Dörfel,[†] Petr Neugebauer,[†] Sebastian Horvath,[‡] Maren Gysler,[†] Theis Brock-Nannestad,[§] Wolfgang Frey,[∥] Michael F. Reid,[‡] and Joris van Slageren*[,†]

[†]Institut für Physikalische Chemie, Universität Stuttgart, Pfaffenwaldring 55, D-70569 Stuttgart, Germany
[‡]Department of Physics and Astronomy, University of Canterbury, Christchurch 8140, New Zealand
[§]Department of Chemistry, University of Copenhagen, Universitetsparken 5, 2100 Copenhagen, Denmark
[∥]Institut für Organische Chemie, Universität Stuttgart, Pfaffenwaldring 55, D-70569 Stuttgart, Germany

Supporting Information

ABSTRACT: The electronic structure of a novel lanthanide-based single-ion magnet, $\{C(NH_2)_3\}_5[Er(CO_3)_4]\cdot 11H_2O$, was comprehensively studied by means of a large number of different spectroscopic techniques, including far-infrared, optical, and magnetic resonance spectroscopies. A thorough analysis, based on crystal field theory, allowed an unambiguous determination of all relevant free ion and crystal field parameters. We show that inclusion of methods sensitive to the nature of the lowest-energy states is essential to arrive at a correct description of the states that are most relevant for the static and dynamic magnetic properties. The spectroscopic investigations also allowed for a full understanding of the magnetic relaxation processes occurring in this system. Thus, the importance of spectroscopic studies for the improvement of single-molecule magnets is underlined.

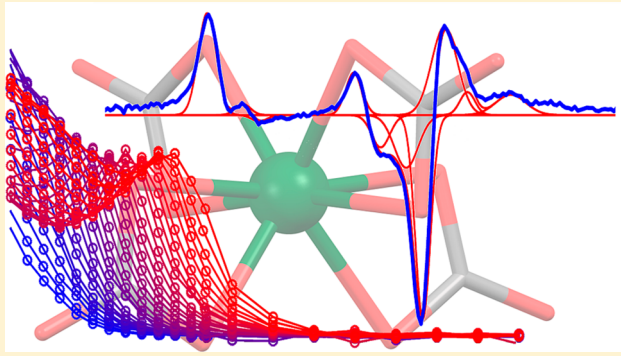

1. INTRODUCTION

The vision that molecules may one day be used to store information at unprecedentedly high densities has been a major driver for research in a number of different areas. In molecular nanomagnetism, it has led to a search for molecules that display magnetic bistability; i.e., their magnetic moments can be either positive or negative and are stable for long periods of time in zero external magnetic field.[1,2] The name single-molecule magnets (SMMs) has been coined for such molecules.[3] Mononuclear SMMs are also known as single-ion magnets (SIMs). The characteristics required are a large magnetic moment and a large magnetic anisotropy that stabilizes states with large z-components of the magnetic moment. Together, these generate an energy barrier toward inversion of the magnetic moment. For polynuclear transition metal complexes, this energy barrier has remained below the 100 K mark.[4] Much larger energy barriers, of up to ca. 1000 K, have been reported for molecular compounds of lanthanide ions, especially of dysprosium(III).[5−7] In lanthanide complexes, the origin of the magnetic anisotropy is the crystal field splitting (CFS) of the microstates of the lowest total angular momentum (J) multiplet. For ions with odd numbers of unpaired electrons (Kramers ions), the minimum degeneracy of the crystal field (CF) states is 2-fold (Kramers doublets) in the absence of an external magnetic field. However, a vast majority of lanthanide complexes do not actually show any magnetic bistability at all, which would be evidenced by sizable coercivity in the magnetic hysteresis curve. The reason for this lack of bistability can be found in the occurrence of efficient underbarrier relaxation processes, such as quantum tunneling. Slowly, strategies are emerging to remedy this issue. First, the implementation of strong magnetic coupling in polynuclear systems can lead to effective quenching of tunneling of the magnetization. For the lanthanides, strong magnetic coupling can only be achieved by means of radical bridging ligands, leading to highly air- and moisture-sensitive species.[8−11] Second, careful engineering of the crystal field (by judicious choice of ligands) can lead to CF eigenstates that are highly "axial", i.e., contain little or no contribution from states with small m_J quantum numbers. As a consequence all transitions between microstates with opposite orientations of the magnetic moment are strongly suppressed.[12] One method to create a strongly axial crystal field is by the use of only two ligands that are placed strictly *trans* to each other.[13,14] This is quite a formidable synthetic challenge. Fortunately, complexes with lower symmetries can also possess axial CF eigenstates,[12,15] and bistability has been found in mononuclear complexes.[16] To make rational progress toward

Received: August 7, 2015
Published: September 22, 2015

ACS Publications © 2015 American Chemical Society

DOI: 10.1021/jacs.5b08344
J. Am. Chem. Soc. 2015, 137, 13114−13120

improving magnetic bistability in lanthanide-based SMMs, the electronic structure and its relation to the molecular structure needs to be understood much better, because the bistability is critically dependent on the detailed nature of the CF eigenstates. So far, all attempts to design novel materials have been based on *ab initio* calculations, and more in-depth experimental study of the CFS is clearly warranted. A second, more technical reason for detailed study of the CFS is for the fit of the temperature dependence of the relaxation time. Often, the high-temperature part of the curve is fit to an exponential function. However, only one (Orbach) of the possible relaxation mechanisms (tunneling, direct, Orbach, and Raman processes) actually has an exponential temperature dependence. Indeed the experimentally derived effective energy barrier often does not correspond to the energy gap to an existing excited CF state as determined by *ab initio* calculations. Because both magnetometry and *ab initio* calculations have finite accuracies,[17] the origins of this discrepancy remain unclear.

Attempts to determine the CFS parameters from powder SQUID magnetometry invariably lead to hopelessly overparametrized situations. Although advanced magnetic measurement methods such as single crystal SQUID and torque magnetometries yield some information on the CFS,[18,19] in-depth information can only be gained from spectroscopic measurements. For these reasons, an increase in spectroscopic measurements has been called for in recent literature.[20,21] A number of spectroscopic methods have been used to study the crystal field splitting in lanthanide SMMs, such as electron paramagnetic resonance,[22−24] far-infrared spectroscopy,[17,23,25] inelastic neutron scattering,[26−28] and luminescence spectroscopy.[29−33] All these studies have been limited to the Russell−Saunders ground multiplet. From these studies, an accurate estimate of the gap between the ground and first excited microstates may be obtained. However, for a detailed understanding of the *nature* of the CF eigenstates, investigation of the ground multiplet alone does not suffice.[34] The precise composition of the lowest CF eigenstates determines the static and dynamic magnetic properties of lanthanide SIMs. Of particular importance is that some CF parameters are highly sensitive to the energies of specific transitions that do not necessarily end in the ground multiplet. Investigation of all the states arising from the $4f^n$ configuration of the lanthanide ion requires extensive spectroscopic measurements, where not only transitions that end in the ground multiplet are considered.

Here we present the first such in-depth spectroscopic investigation of the CF splitting in a lanthanide-based SIM. We employ a combination of far-infrared, magnetic circular dichroism, optical absorption, luminescence, and multifrequency EPR spectroscopies. We have elected to investigate the novel SIM $\{C(NH_2)_3\}_5[Er(CO_3)_4]\cdot 11H_2O$ (**1**),[35] because there are no ligand-based or charge-transfer transitions in the near-UV, visible, or near-infrared regions of the spectrum. Ligand-based transitions precluded in-depth investigations in the case of the complexes $(NBu_4)[LnPc_2]$.[17] We demonstrate that a comprehensive determination of the CFS and the nature of the eigenstates can be achieved in this manner. This allows for a full understanding of the processes relevant for the relaxation of the magnetization.

2. EXPERIMENTAL METHODS

Synthesis of 1. $\{C(NH_2)_3\}_5[Er(CO_3)_4]\cdot 11H_2O$ (**1**) was synthesized according to a slightly modified literature procedure.[35] Guanidine carbonate (9.016 g, 50.0 mmol) was dissolved in 20 mL of doubly distilled water, giving a saturated solution. To this was added $Er(NO_3)_3\cdot 5H_2O$ (1.099 g, 2.5 mmol) in doubly distilled water. A white precipitate formed which was filtered off using a 0.45 μm syringe filter, and the resulting clear solution was stored at 5 °C yielding pale pink crystals after several weeks. Elemental analysis: found (calcd for $C_9H_{52}ErN_{15}O_{23}$)/%: C 11.97 (11.93), H 5.80 (5.79), N 23.12 (23.19). Further characterization data can be found in the Supporting Information.

Magnetic and Spectroscopic Measurements. Magnetic measurements were performed using a Quantum Design MPMS-XL7 SQUID magnetometer. Far-infrared (FIR) spectra were recorded on a Bruker IFS 113v FTIR spectrometer equipped with an Oxford Instruments Spectromag SM4000 optical cryomagnet and an Infrared Laboratories pumped Si bolometer. Optical absorption and magnetic circular dichroism (MCD) spectra were recorded on samples of **1** dispersed into Baysilone vacuum grease on an Aviv 42 CD spectrometer equipped with an Oxford instruments Spectromag 10 T optical cryomagnet and photomultiplier and InGaAs detectors. Luminescence spectra were recorded on a Horiba FluoroLog3 luminescence spectrometer equipped with an Oxford Instruments helium flow optical cryostat and photomultiplier and InGaAs detectors. X-Band EPR spectra were recorded on a Bruker EMX EPR spectrometer equipped with an Oxford Instruments continuous flow cryostat. High-frequency EPR (HFEPR) spectra were recorded on a home-built spectrometer featuring an Anritsu signal generator, a VDI amplifier-multiplier chain, a Thomas Keating quasioptical bridge, an Oxford Instruments 15/17 T solenoid cryomagnet, and a QMC Instruments InSb hot electron bolometer.

Analysis and Calculations. Magnetic data were corrected for diamagnetic contributions using Pascal's constants,[36] and simulations were performed using the simulation software CONDON.[37] The crystal field analysis was carried out by means of the f-shell program package.[38] The program pycf was used to calculate g tensors from the f-shell output.[39] EPR spectra were simulated by using the Easyspin program.[40] The reported uncertainty values were estimated in the following manner: We have taken the standard deviations given by the output of the f-shell program, and modified these by assessing the effect of parameter value modification on the EPR spectra, to give realistic estimates of the parameter uncertainties.

3. RESULTS AND DISCUSSION

Complex **1** was synthesized by means of a facile reaction between aqueous solutions of guanidinium carbonate and erbium(III) nitrate pentahydrate,[35] and characterized by conventional methods (Figure S 1, Figure S 3, Table S 1). X-ray crystallographic analysis (Figure 1, Table S 2) reveals that **1** crystallizes as a hendecahydrate in the monoclinic space group $P2_1/n$, forming a hydrogen bonded network. The $[Er(CO_3)_4]^{5-}$ anion has C_1 site symmetry. To assess the presence of any

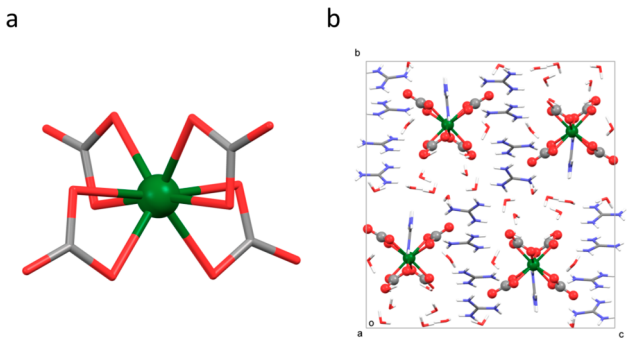

Figure 1. (a) Crystallographically determined molecular structure of the $[Er(CO_3)_4]^{5-}$ anion of **1** viewed perpendicularly to the pseudo-C_2-axis. (b) Packing diagram of **1**: erbium, dark green; oxygen, red; nitrogen, blue; carbon, gray; hydrogen, white.

DOI: 10.1021/jacs.5b08344
J. Am. Chem. Soc. 2015, 137, 13114−13120

approximate higher symmetry, it is helpful to consider the distances between the carbonate carbon atoms. For perfect tetrahedral symmetry, all these distances should be equal. In practice three sets of distances are found (Figure S 2, all distances in Å): 3.970/4.030, 4.318/4.352, 5.043/5.069. Hence, the approximate symmetry of the coordination geometry is C_{2v}, and we have used this symmetry for the analysis of the spectroscopic data (see below). The real symmetry is not only determined by the positions of the coordinating atoms, but also by the rest of the ligand.[17,41] In C_{2v} symmetry the CF is parametrized by 9 independent parameters (see below).[42]

We carried out a magnetic characterization of **1** by means of comprehensive direct current (dc) and alternating current (ac) magnetic susceptibility and magnetization measurements. The dc χT value of **1** is χT = 10.82 cm^3 K mol^{-1} at room temperature (*cf.* the $^4I_{15/2}$ free ion value of 11.48 cm^3 K mol^{-1}), decreasing to 3.75 cm^3 K mol^{-1} at low temperatures (Figure 2).

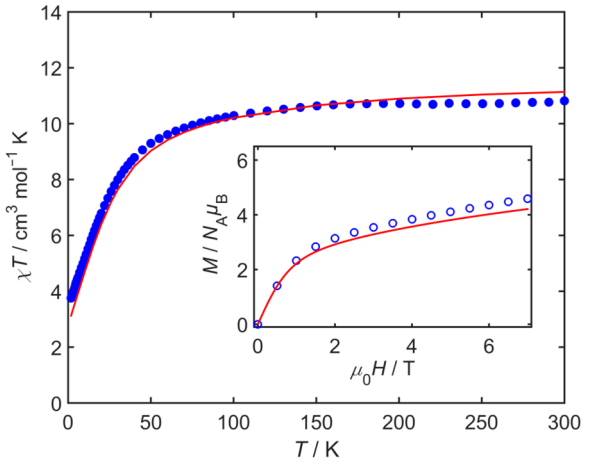

Figure 2. Product of magnetic susceptibility and temperature (χT) as a function of temperature, recorded on a powder pellet of **1** mixed with a minimal amount of vacuum grease, at an applied field of 1000 Oe. The inset shows the magnetization curve recorded on the same sample at 1.8 K. Symbols are experimental data, and solid lines are simulations (see text).

We attribute this decrease to the influence of the CFS of the $^4I_{15/2}$ Russell–Saunders ground multiplet of erbium(III). The molecular magnetization reaches a value of 4.59 μ_B at 1.8 K and 7 T. Without spectroscopic data, attempts to extract the 9 CF parameters from these data would not be fruitful. Alternating susceptibility measurements in an applied field of H_{dc} = 1000 Oe display a clear out-of-phase susceptibility signal (Figure S 4), proving that **1** is a (field induced) SIM. Extensive ac measurements at different frequencies and temperatures (Figure S 5) enabled us to generate Argand plots of the out-of-phase (χ'') as a function of the in-phase component (χ') of the ac susceptibility (Figure 3). The two clearly visible semicircles reveal the presence of two distinct relaxation processes. These data were fitted with generalized Debye equations to extract relaxation times and their distributions (Table S 3). The distribution of relaxation times of the fast process is rather broad (α = 0.1 to α = 0.3), but that of the slow process is quite narrow ($\alpha \leq 0.04$). The relaxation times extracted are displayed as an Arrhenius plot of ln τ as a function of inverse temperature T^{-1} (Figure 4), resulting in a strongly curved dependence for the slow process, and a largely temperature independent fast

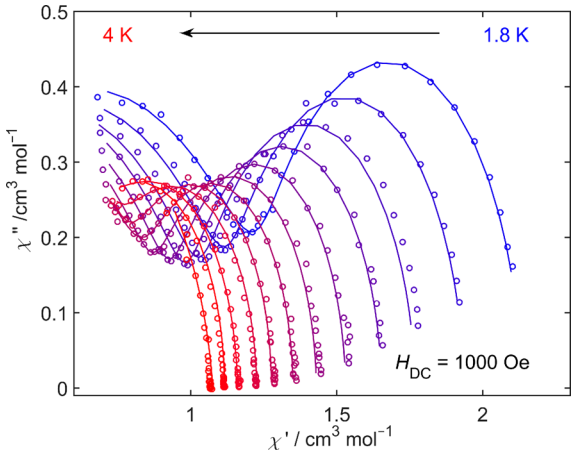

Figure 3. Argand diagram of the out-of-phase component of the alternating current (ac) susceptibility (χ'') as a function of the real component (χ') derived from measurements at different temperatures as indicated. Symbols are experimental data points; lines are fits (see text).

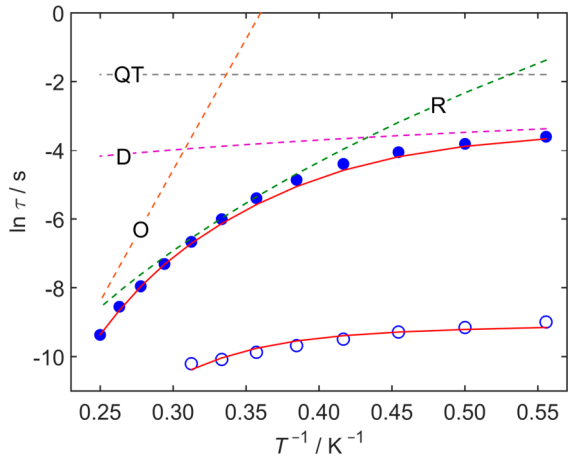

Figure 4. Arrhenius plot of ln τ as a function of T^{-1}. Filled symbols are points derived from experimental data for the slow relaxation process; open symbols are for the fast relaxation process. Dashed lines are the different contributions to the slow relaxation process: D = direct, O = Orbach, QT = quantum tunnelling, R = Raman. The solid line is the sum of these contributions.

process. The temperature dependence of the four relaxation mechanisms is given by eq 1:[43]

$$\tau^{-1} = \underbrace{\frac{B_1}{1 + B_2 H^2}}_{\text{tunneling}} + \underbrace{AH^{n_1}T}_{\text{direct}} + \underbrace{CT^{n_2}}_{\text{Raman}} + \underbrace{\tau_0^{-1}\exp(-\Delta_{CF}/k_B T)}_{\text{Orbach}} \quad (1)$$

Here H is the applied field, and T is the temperature. The parameters B_1, B_2, A, C, and τ_0 all cannot be determined by other than purely empirical means. For the parameters n_1 and n_2, explicit values have been derived for different conditions,[44] but other values are also regularly reported.[45,46] The parameter Δ_{CF} is a real intermediate CF state, typically the first or second, or, in a few cases, higher CF excited state.[47,48] Clearly, this is a severely overparametrized problem. By working at very low temperatures (in practice at T = 1.8 K), it can be assumed that the two-phonon processes (Raman, Orbach) are not operative.

DOI: 10.1021/jacs.5b08344
J. Am. Chem. Soc. 2015, 137, 13114–13120

From the dc field dependence of the relaxation rate at T = 1.8 K (Figure S 6, Figure S 7, Figure S 8, Table S 4), we have derived the parameter values A = 1621 T^{-2} K^{-1} s^{-1}, B_1 = 25.2 s^{-1}, B_2 = 318 T^{-2} for the slow process and $A = 19 \times 10^4$ T^{-2} K^{-1} s^{-1}, $B_1 = 50 \times 10^{15}$ s^{-1}, $B_2 = 3 \times 10^{14}$ T^{-2} for the fast process. Here n_1 has been fixed to the theoretical value of $n_1 = 2$ for a Kramers doublet in the presence of hyperfine interactions.[44] No sensible straight line can be drawn through the points in Figure 4; consequently, the remaining parameters C, n_2, τ_0, and Δ_{CF} cannot be unequivocally determined at this stage. As will be shown below, the first CF excited doublet is located at 52 cm^{-1}. Using this as the value for Δ_{CF} and fixing n_2 to the value derived for Kramers ions in the low-temperature limit (n_2 = 9), we find the following parameter values: C = 0.57 K^{-9} s^{-1} and $\tau_0 = 0$ for the fast process and C = 0.02 K^{-9} s^{-1} and $\tau_0 = 1.2 \times 10^{-12}$ s for the slow process.

To find out the exact composition of the eigenstates that determine the static and dynamic properties and to determine the energies of the CF levels (Δ_{CF}), we have embarked on an extensive spectroscopic study of **1**. First, we have recorded far-infrared (FIR) spectra at 9 K and at different magnetic fields (Figure S 9). The application of an external field allows separating the field dependent CF excitations from field independent excitations such as vibrations that occur in the same frequency range. The CF excitations can be made more evident by normalization of the spectra by division of the in-field spectra by the 6 T spectrum. We observed three CF excitations, namely, at 52, 84, and 105 cm^{-1}. The splitting of the middle feature is an artifact, which we have observed more often in FIR spectra whenever CF and vibrational transitions overlap. The last of these is at the edge of our spectral window, and the assignment to a CF transition on the basis of this measurement alone would not be beyond doubt. However, the CF analysis (see below) shows that there must be a CF level at this position, and we have therefore used this energy.

Luminescence spectroscopy is a second method that furnishes information on the CFS of the ground multiplet. Erbium(III) is well-known for the near-infrared (NIR) luminescent transition from the $^4I_{13/2}$ first excited to the $^4I_{15/2}$ ground multiplet,[49] used in fiber optic telecommunication amplifiers, but also transitions from higher lying states to the ground multiplet occur.[50] However, the low-temperature emission spectrum of **1** (λ_{exc} = 290 nm) merely showed a broad emission band attributed to ligand luminescence. Intriguingly, superimposed on this broad luminescence band are sharp dips, whose energies correspond to the optical absorption bands (Figure S 10). This phenomenon has been observed before,[51,52] and we attribute this to resonant reabsorption of the ligand emission by the lanthanide ion. No ff-luminescence in the visible or near-infrared was observed for any excitation wavelength.

We were, however, able to record a wealth of UV−vis−NIR-absorption and -MCD-spectra (Figure 5, Figures S 11−20). We obtained best results for samples dispersed into transparent vacuum grease. The absorption spectra were calibrated against pure vacuum grease. Because the MCD signal is a signed quantity, often a higher resolution than in the corresponding absorption spectrum is achieved. In absorption, we have observed CF split transitions from the $^4I_{15/2}$ ground state to the $^4I_{9/2}$, $^4F_{9/2}$, $^4S_{3/2}$, $^2H_{11/2}$, $^4F_{7/2}$, $^4F_{5/2}$, $^4F_{3/2}$, $^2H_{9/2}$, and $^4G_{11/2}$ multiplets, whereas MCD spectra allowed the observation of transitions to $^4I_{13/2}$, $^4F_{9/2}$, $^2H_{11/2}$, $^4F_{7/2}$, $^4F_{5/2}$, $^4F_{3/2}$, and $^4H_{11/2}$.[53] Further transitions were observed, but either they were too weak or no usable CF splitting was observed, so they were not taken into account in the analysis. All spectra were carefully deconvoluted into sums of Gaussian lines. Often more lines would be observed than expected on the basis of the multiplicity of the final state. These are attributed to vibronic excitations that occur because ff electric dipole transitions are Laporte-forbidden, and can gain intensity through coupling with ungerade vibrational modes.[42] In the analysis, we have almost always used the lower-energy component. From the FIR and optical data together, we were able to determine the positions of no fewer than 48 independent energy levels (Table S 5).

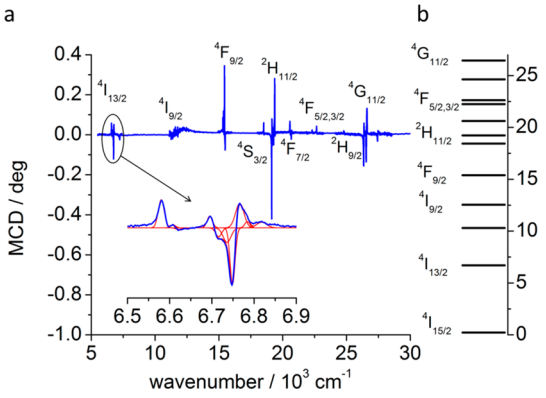

Figure 5. (a) Complete magnetic circular dichroism (MCD) spectrum, composed of several separate scans, recorded on a mull of **1** in transparent vacuum grease. The inset shows a zoom of the $^4I_{15/2} \rightarrow {}^4I_{13/2}$ transition. (b) Energy level diagram showing the calculated energetic positions (in 10^3 cm^{-1}) of the multiplets.

For the magnetic properties, the lowest-lying Kramers doublets (KDs) are of the most interest. A technique that can be exquisitely sensitive to the precise composition of the lowest KDs is (high-frequency) EPR.[23] We have therefore recorded EPR spectra on **1** at X-band (9.5 GHz) and at high frequencies around 300 GHz (Figure 6). Especially in the latter,

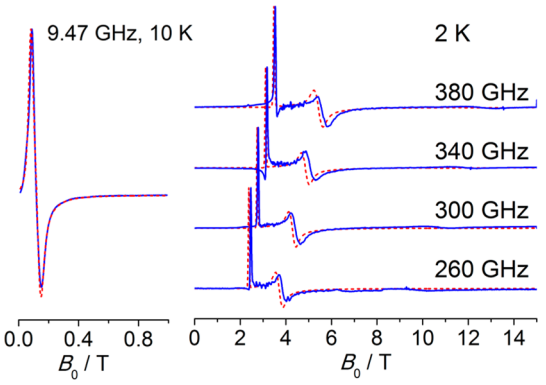

Figure 6. Experimental (blue, solid) and simulated (red, dashed) X-band EPR (left, 10 K) and high-frequency EPR (right, 2 K) spectra recorded on mulls of **1** in Fluorolube.

two clear and one weaker resonance line can be clearly observed. Within the $S = {}^1/_2$ pseudospin approximation we find effective g-values g_1 = 7.64, g_2 = 4.85, and g_3 = 1.94.

The Hamiltonian that describes the electronic structure of a C_{2v}-symmetric lanthanide complex in the space of the $4f^n$ configuration is given in eq 2:[42]

DOI: 10.1021/jacs.5b08344
J. Am. Chem. Soc. 2015, 137, 13114−13120

$$\mathcal{H} = \mathcal{H}_{\text{free ion}} + \mathcal{H}_{\text{crystal field}}$$

$$\mathcal{H}_{\text{free ion}} = E_{\text{ave}} + \sum_{k=2,4,6} F^k f_k + \zeta_{4f} A_{SO} + \alpha L(L+1) + \beta G(G_2) + \gamma G(R_7) + \sum_{i=2,3,4,6,7,8} T^i t_i + \sum_l M^l m_l + \sum_k P^k p_k$$

$$\mathcal{H}_{\text{crystal field}} = -e[B_{20}C_0^2 + B_{22}(C_{-2}^2 + C_2^2) + B_{40}C_0^4 + B_{42}(C_{-2}^4 + C_2^4) + B_{44}(C_{-4}^4 + C_4^4) + B_{60}C_0^6 + B_{62}(C_{-2}^6 + C_2^6) + B_{64}(C_{-4}^6 + C_4^6) + B_{66}(C_{-6}^6 + C_6^6)] \quad (2)$$

Here E_{ave} is the spherical contribution to the energy, $F^k f_k$ are the electrostatic repulsion integrals, and ζ_{4f} is the spin−orbit coupling constant. The remaining terms of $\mathcal{H}_{\text{free ion}}$ are two and three particle, as well as spin−spin and spin−orbit corrections. These parameters have little influence on the spectroscopically observed splittings and were fixed to literature mean values during the fitting procedure.[42] The crystal field Hamiltonian $\mathcal{H}_{\text{crystal field}}$ is expressed in the Wybourne notation. Here, B_{kq} are the adjustable parameters, and C_q^k are spherical tensor operators. Note that C_q^k are not formulated in terms of the Stevens operators typical for analyses in the basis of the Russell−Saunders ground multiplet. We have used this Hamiltonian in the full basis of all 364 states arising from the $4f^{11}$ configuration.

The fit followed the following procedure: First, the experimentally determined data (FIR, optical absorption, MCD) were ranked according to energy. In case more excitations were observed than expected on the basis of the multiplicity of the relevant final state, some excitations were tentatively assigned to vibronic excitations and temporarily discarded. Subsequently, the 14 parameters were fit to these levels. On the basis of the results, the energy levels were reassigned, and the process was repeated in the search of the global minimum. Once a reasonable fit (root-mean-square error less than 20 cm^{-1}) was obtained, its quality was assessed by simulating the HFEPR spectra on the basis of this parameter set. After a lengthy iterative process, we finally arrived at a robust and consistent parameter set (parameter set 1, Table 1), with a final rms error of ca. 17 cm^{-1} (Table S 5), which also allows excellent simulations of the susceptibility, magnetization, and HFEPR data (Figure 2, Figure 6). The obtained parameters were transformed, so that they lie in the standard range for which $0 \le B_{22}/B_{20} \le (1/6)^{1/2}$.[54] The deviations of the energies of the KDs of the ground multiplet with those directly measured by FIR spectroscopy are less than 10 cm^{-1} (Table 2).

Table 1. Free Ion and Crystal Field Parameters Derived for 1

param	value/cm^{-1}
E_{ave}	35 469 ± 10
F^2	95 991 ± 100
F^4	69 046 ± 105
F^6	51 686 ± 170
ζ_{4f}	2355 ± 2
B_{20}	145 ± 50
B_{22}	40 ± 25
B_{40}	0 ± 50
B_{42}	930 ± 30
B_{44}	−386 ± 30
B_{60}	350 ± 30
B_{62}	440 ± 20
B_{64}	620 ± 15
B_{66}	330 ± 50

Table 2. Energies of the Lowest $^4I_{15/2}$ Multiplet Directly Measured by FIR Spectroscopy and Those Derived from the Crystal Field Analysis

E_{exp}/cm^{-1} (FIR)	E_{CF}/cm^{-1}
0	0
52	44
84	91
105	112
	280
	325
	437
	462

We can now inspect the composition of the ground KD (Table S 6), which is decisive for the low-temperature magnetic properties. Although we have carried out the analysis in the complete basis of the $4f^{11}$ configuration, we find that the ground KD only contains contributions from the $^4I_{15/2}$ Russell−Saunders ground multiplet: $|KD1\rangle = \sum c_i|^{2S+1}L_J\ m_J\rangle_i = \sum c_i|m_J\rangle_i = 0.50|-13/2\rangle - 0.50|-5/2\rangle + 0.42|11/2\rangle - 0.36|3/2\rangle - 0.27|15/2\rangle - 0.27|-1/2\rangle - 0.20|-9/2\rangle$, with the second component of the doublet the mirror image of the first. Hence, the ground Kramers doublet is extraordinarily mixed in character and contains contributions from functions with low m_J values, and also contributions with both positive and negative m_J components. This leads to efficient relaxation of the magnetization explaining the relatively poor performance of **1** as a single-molecule magnet.[43] It will be interesting to investigate the crystal field splitting of erbium single molecule magnets where more axial KDs are expected, such as $Er[N(SiMe_3)_2]_3$,[55] by the methodology described in this paper.

An important point is the following: If the CF parameters are fit to the experimentally derived (FIR, optical absorption, MCD) energy levels *without* taking into account the EPR data, a parameter set with a smaller rms error (13 cm^{-1}) can be found (parameter set 2, Table S 8). This parameter set features rather different CF splitting parameters and predicts the ground KD to have smaller contributions from functions with small values of m_J (Table S 9, Figure S 23). However, this parameter set does not allow for reasonable fits of the magnetic and EPR data (Figure S 21, Figure S 22), and therefore must be wrong. This leads to the important conclusion that an analysis of the CF splitting on the basis of optical data alone is not necessarily sufficient to correctly determine the composition of the lowest Kramers doublets that are crucially important for the dc and ac magnetic properties. Similar effects may explain unexpected discrepancies between experimental and calculated susceptibility data reported recently.[21]

CONCLUSIONS

We have presented an in-depth analysis of the magnetic properties and the electronic structure of a novel lanthanide-based single-ion magnet. The study has allowed for a full understanding of the magnetization dynamics. Importantly, we

DOI: 10.1021/jacs.5b08344
J. Am. Chem. Soc. 2015, 137, 13114−13120

have presented the first comprehensive electronic structure determination of a lanthanide single-molecule magnet. We have shown that, for a correct description of the states relevant for the magnetic properties, including the results from electron paramagnetic resonance measurements is crucial. We are convinced that detailed understanding of the electronic structure of lanthanide-based single-molecule magnets, such as that achieved in the present paper, is essential for rational design of novel such systems with improved properties.

■ ASSOCIATED CONTENT

Supporting Information

The Supporting Information is available free of charge on the ACS Publications website at DOI: 10.1021/jacs.5b08344.

Detailed information on synthesis and characterization, equipment used, magnetic and spectroscopic measurements, data analysis, and calculations (PDF)

■ AUTHOR INFORMATION

Corresponding Author

*slageren@ipc.uni-stuttgart.de

Present Address

⊥Max Planck Institute for Chemical Physics of Solids, Nöthnitzer Straße 40, D-01187 Dresden, Germany.

Notes

The authors declare no competing financial interest.

■ ACKNOWLEDGMENTS

We thank Claudio Eisele (University of Stuttgart) for experimental contributions, Pierre Eckold (University of Stuttgart) for powder X-ray diffraction measurements, Martin Dressel (University of Stuttgart) for access to the SQUID magnetometer and FIR spectrometer, George S. Goff (Los Alamos National Laboratory) for useful discussions, as well as DFG (INST 41/863-1, 41/864-1, SPP1601, SL104/5-1) and COST CM1006 Eufen for funding.

■ REFERENCES

(1) Gatteschi, D.; Sessoli, R.; Villain, J. *Molecular Nanomagnets*; Oxford University Press: Oxford, 2006.

(2) Sessoli, R.; Gatteschi, D.; Caneschi, A.; Novak, M. A. *Nature* **1993**, *365*, 141.

(3) Aubin, S. M. J.; Wemple, M. W.; Adams, D. M.; Tsai, H. L.; Christou, G.; Hendrickson, D. N. *J. Am. Chem. Soc.* **1996**, *118*, 7746.

(4) Milios, C. J.; Vinslava, A.; Wernsdorfer, W.; Moggach, S.; Parsons, S.; Perlepes, S. P.; Christou, G.; Brechin, E. K. *J. Am. Chem. Soc.* **2007**, *129*, 2754.

(5) Woodruff, D. N.; Winpenny, R. E. P.; Layfield, R. A. *Chem. Rev.* **2013**, *113*, 5110.

(6) Ishikawa, N.; Sugita, M.; Ishikawa, T.; Koshihara, S.; Kaizu, Y. *J. Phys. Chem. B* **2004**, *108*, 11265.

(7) Ishikawa, N.; Mizuno, Y.; Takamatsu, S.; Ishikawa, T.; Koshihara, S. Y. *Inorg. Chem.* **2008**, *47*, 10217.

(8) Rinehart, J. D.; Fang, M.; Evans, W. J.; Long, J. R. *J. Am. Chem. Soc.* **2011**, *133*, 14236.

(9) Rinehart, J. D.; Fang, M.; Evans, W. J.; Long, J. R. *Nat. Chem.* **2011**, *3*, 538.

(10) Demir, S.; Zadrozny, J. M.; Nippe, M.; Long, J. R. *J. Am. Chem. Soc.* **2012**, *134*, 18546.

(11) Demir, S.; Nippe, M.; Gonzalez, M. I.; Long, J. R. *Chem. Sci.* **2014**, *5*, 4701.

(12) Ungur, L.; Chibotaru, L. F. *Phys. Chem. Chem. Phys.* **2011**, *13*, 20086.

(13) Chilton, N. F. *Inorg. Chem.* **2015**, *54*, 2097.

(14) Chilton, N. F.; Goodwin, C. A. P.; Mills, D. P.; Winpenny, R. E. P. *Chem. Commun.* **2015**, *51*, 101.

(15) Aravena, D.; Ruiz, E. *Inorg. Chem.* **2013**, *52*, 13770.

(16) Ungur, L.; Le Roy, J. J.; Korobkov, I.; Murugesu, M.; Chibotaru, L. F. *Angew. Chem., Int. Ed.* **2014**, *53*, 4413.

(17) Marx, R.; Moro, F.; Dörfel, M.; Ungur, L.; Waters, M.; Jiang, S. D.; Orlita, M.; Taylor, J.; Frey, W.; Chibotaru, L. F.; van Slageren, J. *Chem. Sci.* **2014**, *5*, 3287.

(18) Cucinotta, G.; Perfetti, M.; Luzon, J.; Etienne, M.; Car, P. E.; Caneschi, A.; Calvez, G.; Bernot, K.; Sessoli, R. *Angew. Chem., Int. Ed.* **2012**, *51*, 1606.

(19) Perfetti, M.; Cucinotta, G.; Boulon, M.-E.; El Hallak, F.; Gao, S.; Sessoli, R. *Chem. - Eur. J.* **2014**, *20*, 14051.

(20) Sorace, L.; Benelli, C.; Gatteschi, D. *Chem. Soc. Rev.* **2011**, *40*, 3092.

(21) Karbowiak, M.; Rudowicz, C.; Ishida, T. *Inorg. Chem.* **2013**, *52*, 13199.

(22) Lucaccini, E.; Sorace, L.; Perfetti, M.; Costes, J.-P.; Sessoli, R. *Chem. Commun.* **2014**, *50*, 1648.

(23) Moreno Pineda, E.; Chilton, N. F.; Marx, R.; Dorfel, M.; Sells, D. O.; Neugebauer, P.; Jiang, S.-D.; Collison, D.; van Slageren, J.; McInnes, E. J. L.; Winpenny, R. E. P. *Nat. Commun.* **2014**, *5*, 5243.

(24) Ghosh, S.; Datta, S.; Friend, L.; Cardona-Serra, S.; Gaita-Ariño, A.; Coronado, E.; Hill, S. *Dalton Trans.* **2012**, *41*, 13697.

(25) Haas, S.; Heintze, E.; Zapf, S.; Gorshunov, B.; Dressel, M.; Bogani, L. *Phys. Rev. B: Condens. Matter Mater. Phys.* **2014**, *89*, 174409.

(26) Pedersen, K. S.; Ungur, L.; Sigrist, M.; Sundt, A.; Schau-Magnussen, M.; Vieru, V.; Mutka, H.; Rols, S.; Weihe, H.; Waldmann, O.; Chibotaru, L. F.; Bendix, J.; Dreiser, J. *Chem. Sci.* **2014**, *5*, 1650.

(27) Kofu, M.; Yamamuro, O.; Kajiwara, T.; Yoshimura, Y.; Nakano, M.; Nakajima, K.; Ohira-Kawamura, S.; Kikuchi, T.; Inamura, Y. *Phys. Rev. B: Condens. Matter Mater. Phys.* **2013**, *88*, 064405.

(28) Klokishner, S. I.; Ostrovsky, S. M.; Reu, O. S.; Palii, A. V.; Tregenna-Piggott, P. L. W.; Brock-Nannestad, T.; Bendix, J.; Mutka, H. *J. Phys. Chem. C* **2009**, *113*, 8573.

(29) Flanagan, B. M.; Bernhardt, P. V.; Krausz, E. R.; Lüthi, S. R.; Riley, M. J. *Inorg. Chem.* **2002**, *41*, 5024.

(30) Long, J.; Rouquette, J.; Thibaud, J.-M.; Ferreira, R. A. S.; Carlos, L. D.; Donnadieu, B.; Vieru, V.; Chibotaru, L. F.; Konczewicz, L.; Haines, J.; Guari, Y.; Larionova, J. *Angew. Chem., Int. Ed.* **2015**, *54*, 2236.

(31) Pointillart, F.; Guennic, B. L.; Maury, O.; Golhen, S.; Cador, O.; Ouahab, L. *Inorg. Chem.* **2013**, *52*, 1398.

(32) Shintoyo, S.; Murakami, K.; Fujinami, T.; Matsumoto, N.; Mochida, N.; Ishida, T.; Sunatsuki, Y.; Watanabe, M.; Tsuchimoto, M.; Mrozinski, J.; Coletti, C.; Re, N. *Inorg. Chem.* **2014**, *53*, 10359.

(33) Pedersen, K. S.; Dreiser, J.; Weihe, H.; Sibille, R.; Johannesen, H. V.; Sørensen, M. A.; Nielsen, B. E.; Sigrist, M.; Mutka, H.; Rols, S.; Bendix, J.; Piligkos, S. *Inorg. Chem.* **2015**, *54*, 7600.

(34) Karbowiak, M.; Rudowicz, C. *Polyhedron* **2015**, *93*, 91.

(35) Goff, G. S.; Cisneros, M. R.; Kluk, C.; Williamson, K.; Scott, B.; Reilly, S.; Runde, W. *Inorg. Chem.* **2010**, *49*, 6558.

(36) Bain, G. A.; Berry, J. F. *J. Chem. Educ.* **2008**, *85*, 532.

(37) Schilder, H.; Lueken, H. *J. Magn. Magn. Mater.* **2004**, *281*, 17.

(38) Reid, M. F. *F-Shell Empirical Programs*; University of Canterbury: Christchurch, New Zealand.

(39) Horvath, S.; Reid, M. F. *pcyf*; https://bitbucket.org/sebastianhorvath/pycf/, 2015.

(40) Stoll, S.; Schweiger, A. *J. Magn. Reson.* **2006**, *178*, 42.

(41) Petit, S.; Pilet, G.; Luneau, D.; Chibotaru, L. F.; Ungur, L. *Dalton Trans.* **2007**, 4582.

(42) Görller-Walrand, C.; Binnemans, K. In *Handbook on the Physics and Chemistry of Rare Earths*; Gschneidner, K. A., Eyring, L., Eds.; Elsevier: Amsterdam, 1996; Vol. 23.

(43) Liddle, S. T.; van Slageren, J. *Chem. Soc. Rev.* **2015**, *44*, 6655.

(44) Abragam, A.; Bleany, B. *Electron Paramagnetic Resonance of Transition Ions*; Dover Publications, Inc.: New York, 1986.

DOI: 10.1021/jacs.5b08344
J. Am. Chem. Soc. 2015, 137, 13114−13120

(45) Boulon, M. E.; Cucinotta, G.; Luzon, J.; Degl'Innocenti, C.; Perfetti, M.; Bernot, K.; Calvez, G.; Caneschi, A.; Sessoli, R. *Angew. Chem., Int. Ed.* **2013**, *52*, 350.
(46) Herchel, R.; Váhovská, L.; Potočňák, I.; Trávníček, Z. *Inorg. Chem.* **2014**, *53*, 5896.
(47) Blagg, R. J.; Ungur, L.; Tuna, F.; Speak, J.; Comar, P.; Collison, D.; Wernsdorfer, W.; McInnes, E. J. L.; Chibotaru, L. F.; Winpenny, R. E. P. *Nat. Chem.* **2013**, *5*, 673.
(48) Singh, S. K.; Gupta, T.; Shanmugam, M.; Rajaraman, G. *Chem. Commun.* **2014**, *50*, 15513.
(49) Comby, S.; Bünzli, J. C. G. In *Handbook on the Physics and Chemistry of Rare Earths, Vol 37: Optical Spectroscopy*; Gschneidner, K. A., Bünzli, J.-C. G., Pecharsky, V. K., Eds.; Elsevier: Amsterdam, 2007; Vol. 37, p 217.
(50) Bünzli, J.-C. G. *Chem. Rev.* **2010**, *110*, 2729.
(51) Kang, J. G.; Kim, T. J.; Park, K. S.; Kang, S. K. *Bull. Korean Chem. Soc.* **2004**, *25*, 373.
(52) Martín-Ramos, P.; Coutinho, J. T.; Ramos Silva, M.; Pereira, L. C. J.; Lahoz, F.; da Silva, P. S. P.; Lavin, V.; Martín-Gil, J. *New J. Chem.* **2015**, *39*, 1703.
(53) Dieke, G. H. *Spectra and Energy Levels of Rare Earth Ions in Crystals*; Interscience Publishers: New York, 1968.
(54) Rudowicz, C.; Chua, M.; Reid, M. F. *Phys. B* **2000**, *291*, 327.
(55) Zhang, P.; Zhang, L.; Wang, C.; Xue, S. F.; Lin, S. Y.; Tang, J. K. *J. Am. Chem. Soc.* **2014**, *136*, 4484.

DOI: 10.1021/jacs.5b08344
J. Am. Chem. Soc. 2015, 137, 13114−13120